Experimental and theoretical threshold photoelectron spectra of methylene

L. Coudert, B. Gans, F. Holzmeier, J.-C. Loison, G. Garcia, C. Alcaraz, A. Lopes, A. Röder

Experimental and theoretical threshold photoelectron spectra of methylene

Laurent H. Coudert,[1, a)] Bérenger Gans,[1] F. Holzmeier,[2, b)] Jean-Christophe Loison,[3] G. A. Garcia,[4] C. Alcaraz,[5] A. Lopes,[5] and A. Röder[6, b)]

[1)] *Institut des Sciences Moléculaires d'Orsay (ISMO), CNRS, Univ. Paris-Sud, Université Paris-Saclay, F-91405 Orsay cedex, France*

[2)] *Dipartimento di Fisica, Politecnico di Milano, 20133 Milano, Italy*

[3)] *Institut des Sciences Moléculaires, UMR 5255 CNRS - Université de Bordeaux, Bât. A12, 351 Cours de la Libération, F-33405 Talence cedex, France*

[4)] *L'Orme des Merisiers; Saint Aubin BP 48, Synchrotron SOLEIL, Gif sur Yvette, France*

[5)] *Laboratoire de Chimie Physique, UMR 8000 CNRS - Université Paris-Sud et Université Paris-Saclay, Bât. 350, F-91405 Orsay cedex, France*

[6)] *Department of Chemistry and Biomolecular Sciences, University of Ottawa, 10 Marie Curie, K1N 6N5 Ottawa, Canada*

(Dated: 5 November 2018)

The threshold photoelectron spectrum of methylene (CH_2), produced by consecutive H atom abstractions on methane, has been recorded using synchrotron radiation. The experimental spectrum spans the region of the $X^+\,^2\Pi_u \leftarrow X\,^3B_1$ ionizing transition. It is modeled starting from *ab initio* bending potentials and using the bending approach introduced by Coudert *et al.* [*J. Chem. Phys.* **148,** 054302 (2018)] accounting for the quasilinearity of CH_2 and the strong Renner-Teller interaction in CH_2^+. This first calculation yields a theoretical threshold photoelectron spectrum which is in moderate agreement with the experimental one. A more accurate approach treating the three vibrational modes is developed for computing the threshold photoelectron spectrum of triatomic C_{2v} molecules. This new treatment is tested modeling the already measured threshold photoelectron spectrum of the $X^+\,^2\Pi_u \leftarrow X\,^1A_1$ ionizing transition of the water molecule. The threshold photoelectron spectrum of CH_2 computed with the new approach compares more favorably with the experimental spectrum and yields an adiabatic ionization potential of 10.386(6) eV.

I. INTRODUCTION

Methylene (CH_2) is an open-shell molecule with a triplet $X\,^3B_1$ ground electronic state.[1,2] Its photoion yield was recorded almost 20 years ago[3,4] providing us with a value of its adiabatic ionization energy ranging from 10.393(11) to 10.3962(36) eV. More recently, its threshold photoionization spectrum was recorded using pulsed-field-ionization zero-kinetic-energy (PFI-ZEKE) photoelectron spectroscopy.[5,6] A rotationally resolved spectrum containing the $X^+\,^2A_1 \leftarrow X\,^3B_1$ ionizing transition was recorded from 10.3 to 10.4 eV and analyzed yielding rotational constants for CH_2^+ and a more accurate value of 10.3864(4) eV for the adiabatic ionization potential. As methylene is already spectroscopically characterized,[7–13] this spectrum provided us with information about low lying rotational levels of the elusive CH_2^+ cation.[14] Except for the ν_3 band reported by Rösslein *et al.*[15] and the vibronic bands reported by Oka and coworkers,[16,17] the cation still is spectroscopically poorly characterized.

In this study the threshold photoelectron spectrum (TPES) of CH_2 has been recorded from 9.8 to 12 eV using a recently developed flow tube reactor[18,19] and VUV synchrotron radiation.[20] The spectrum spans a larger energy range than that previously reported,[5,6] but with a lower resolution. It displays narrow and broad features due to the $X^+\,^2A_1 \leftarrow X\,^3B_1$ and $A^+\,^2B_1 \leftarrow X\,^3B_1$ ionizing transitions, respectively. Modeling this spectrum is challenging as it requires accounting for the quasilinearity[21,22] of the neutral, due to the coupling between the large amplitude bending mode and the overall rotation,[13] and for the strong Renner-Teller interaction in the $^2\Pi_u$ ground electronic state of the cation leading to the lower $X^+\,^2A_1$ and the upper $A^+\,^2B_1$ electronic substates.

Starting from new *ab initio* bending potentials, the photoelectron spectrum has been modeled with the bending approach of Coudert *et al.*[23] accounting for the quasilinearity of the neutral and for the Renner-Teller interaction in the cation. The spectrum has also been computed with a new model in which all three vibrational modes are treated, the tridimensional Schrödinger equation being solved with the help of Radau coordinates[24] and the Renner-Teller effects in the cation described using the rovibronic Hamiltonian of Mitrushchenkov.[25] This tridimensional model, more satisfactory than the bending one[23] from the physical point of view, allows us to obtain all the vibrational states of the neutral and the cation and is expected to lead to a better agreement with the experimental spectrum. With the help of tridimensional potential energy surfaces[26,27] available for H_2O and H_2O^+, this new model is first tested computing the TPES of the $X^+\,^2\Pi_u \leftarrow X\,^1A_1$ ionizing transition of the water

[a)] Electronic mail: laurent.coudert@u-psud.fr

[b)] This research was performed while at Institute for Physical and Theoretical Chemistry, University of Würzburg, 97074 Würzburg, Germany

molecule, used here to validate the model. Based on the multidimensional potential energy surfaces[28–31] available for CH_2 and CH_2^+, the new model is then used for computing the TPES of CH_2 and analyzing the experimental TPES recorded in this work. The agreement is more satisfactory than with the bending approach.[23]

The paper has four remaining sections. In Section II, the experimental method used to produce methylene is described along with the recording of the TPES. Section III reports on the spectrum calculated with the bending approach. In Section IV, the tridimensional approach is introduced and applied to the calculation of the water molecule and methylene TPES, which are compared to experimental data. Section V is the discussion.

II. EXPERIMENTAL TPES

The experimental results presented in this paper have been obtained on the DESIRS beamline[20] at synchrotron SOLEIL. The experimental setup has been described previously.[18,19] Briefly, the radicals are produced in a flow tube reactor by consecutive H atom abstractions through chemical reactions of a precursor and atomic fluorine. After the photoionization of the radicals by the monochromatized synchrotron radiation, the resulting photoelectrons and photoions were analyzed with the DELICIOUS III spectrometer.[32]

The methylene spectrum has been recorded simultaneously with that of the CH radical presented elsewhere.[33] Experimental conditions should be found in this reference. Both species were produced by consecutive H atom abstractions on methane. The TPES spectrum resolution was 17 meV (137 cm^{-1}) and the absolute accuracy of the energy scale was found to be 3.2 meV. Note that the 35 V/cm DC field used to extract the photoelectron and the photoion resulted in a field-induced shift of the CH_2 ionization potential of about -4.4 ± 1.0 meV. The final absolute accuracy on ionization threshold measurements was about 4 meV. The experimental TPES is shown in Fig. 1 and consists of a narrow isolated feature at 10.38 eV and a broader feature spanning the 10.6 to 12 eV energy range where 9 bands can be seen at 10.74, 10.88, 11.03, 11.16, 11.31, 11.47, 11.61, 11.75, and 11.89 eV. The band at 10.74 eV being the strongest line of the broad feature.

III. BENDING TREATMENT

The threshold photoelectron spectrum of CH_2 is modeled using a slightly modified version of the bending treatment introduced by Coudert *et al.*[23] Starting from *ab initio* calculations, rovibronic energies of CH_2 and CH_2^+ are evaluated accounting for the quasi-linearity of the former and the Renner-Teller effects in the latter. An expression for the total photoionization cross sections is derived using the results of Coudert *et al.*[23]

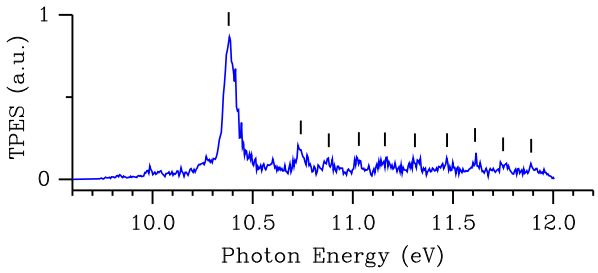

Figure 1. The experimental TPES of the $X^+\,^2\Pi_u \leftarrow X\,^3B_1$ ionizing transition of CH_2 is plotted as a function of the photon energy in eV. Short vertical lines indicate the position of the 10 strongest bands of the spectrum.

A. Ab initio bending potentials

The *ab initio* calculations of the triplet ground electronic state[1,2] of CH_2 ($X\,^3B_1$) and of the two substates ($X^+\,^2A_1$ and $A^+\,^2B_1$) of the $^2\Pi_u$ Renner-Teller split ground electronic state of CH_2^+ were carried out by using the internally contracted multireference configuration interaction method with Davidson correction (MRCI + Q) with complete active space self-consistent field (CASSCF) wavefunctions. All calculations were performed using the MOLPRO program package[34,35] and the Dunning augmented quintuple zeta basis, the energies being corrected for basis set superposition error (BSSE). The potential energy curves of the electronic states were computed as a function of the ∠HCH bending angle, denoted γ, the r(CH) distances being optimized for each angle and each electronic state. The CASSCF and MRCI calculations were performed at full active space, namely with 8 electrons distributed in 7 orbitals with the 1s orbital of the carbon atom kept doubly occupied but fully optimized. These numerical values were least squares fitted to a polynomial-type expansion $F(\gamma)$ written in terms of $\pi-\gamma$, the supplement of γ:

$$F(\gamma)=\sum_{i=0}^{n} f_{2i}(\pi-\gamma)^{2i}, \qquad (1)$$

where f_{2i}, with $0\le i\le n$, are the fitted parameters. Two such sets of parameters, one for the bending potential and one for the bond lengths, were retrieved for the electronic ground state of CH_2. Four such sets of parameters were obtained for the doublet $X^+\,^2A_1$ and $A^+\,^2B_1$ electronic substates of CH_2^+. The f_0 parameters of both substates were constrained to be equal to ensure the required degeneracy for the $\gamma=\pi$ linear configuration. In Eq. (1), n was set to 4 for the bending potentials allowing us to reproduce the *ab initio* values of the $X\,^3B_1$, $X^+\,^2A_1$, and $A^+\,^2B_1$ states with root-mean-square (RMS) deviations of 14, 42, and 29 cm^{-1}, respectively. For the bond lengths, n was set to 3 for the $X\,^3B_1$ state and to 4 for the $X^+\,^2A_1$ and $A^+\,^2B_1$ substates and *ab initio* values were reproduced with RMS deviations of 3.5×10^{-4}, 2.2×10^{-4}, and 0.6×10^{-4} Å, respectively.

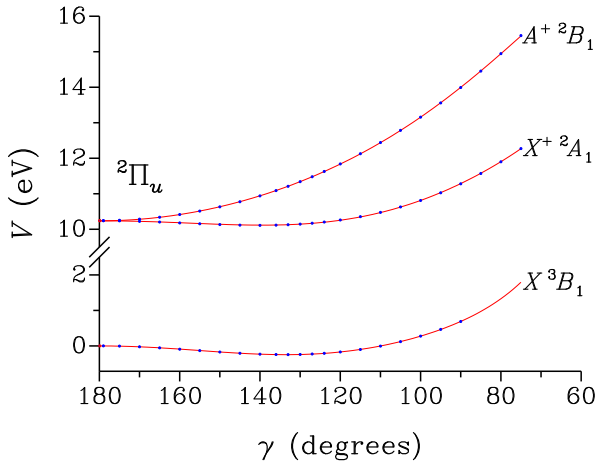

Figure 2. Variations with the bending angle $\gamma = \angle$HCH of the potential energy function V in eV for the $X\,^3B_1$ ground electronic state of methylene and for the $X^+\,^2A_1$ and $A^+\,^2B_1$ substates of the CH_2^+ cation. *Ab initio* potential values are indicated by dots. Solid lines are the fitted bending potentials calculated with Eq. (1).

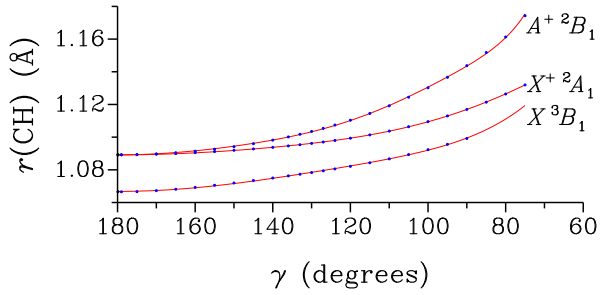

Figure 3. Variations with the bending angle $\gamma = \angle$HCH of the r(CH) bond length in Å for the $X\,^3B_1$ ground electronic state of methylene and for the $X^+\,^2A_1$ and $A^+\,^2B_1$ substates of the CH_2^+ cation. *Ab initio* bond length values are indicated by dots. Solid lines are the fitted bond lengths calculated with Eq. (1).

Figures 2 and 3 show fitted bending potentials and bond lengths, respectively, as well as *ab initio* points. For the ground $X\,^3B_1$ electronic state of methylene, the equilibrium geometry is characterized by a bending angle γ of 133.9° and a value of the r(CH) bond length of 1.077 Å. The linear configuration is 1902 cm^{-1} above this minimum and is characterized by a bond length of 1.067 Å. These values compare well with those characterizing the minimum of the tridimensional potential energy surface retrieved by Jensen and Bunker,[28] 133.93° and 1.075 Å for the bending angle and the bond length, respectively. For the linear configuration, these authors obtained an energy of 1916 cm^{-1} and a bond length of 1.067 Å. For the lower $X^+\,^2A_1$ Renner-Teller substate of the cation, the equilibrium geometry is characterized by $\gamma = 139.2°$ and r(CH) = 1.094 Å. This minimum is 975.7 cm^{-1} below the linear configuration characterized by r(CH) = 1.089 Å. These values should be compared to those reported by Bunker *et al.*[31] for the minimum of their tridimensional potential energy surface, 140.81° and 1.0933 Å, and, for the linear configuration, an energy of 1033 cm^{-1} and a bond length of 1.0889 Å. As Bunker *et al.*,[31] we find that the minimum of the upper $A^+\,^2B_1$ Renner-Teller substate occurs at the linear configuration. The energy difference calculated in this work between the cation and the neutral for the linear geometry is 10.2377 eV.

B. Rovibronic energies

In this calculation, the asymmetry doubling and the spin-rotation and hyperfine couplings are ignored. In the case of the cation, the spin-orbit splitting is also ignored. For the neutral, bending-rotation energies are calculated as in Section III A of Coudert *et al.*[23] The maximum value of n for the basis set functions in Eq. (4) of this reference, $n_{\rm Max}$, is set to 33, α the parameter describing these basis set functions, to 10, and P the Gauss-Jacobi quadrature number of points, to 33. Symmetry adapted rovibrational wavefunctions appropriate for the C_{2v} symmetry group can be obtained from Eq. (11) of Coudert *et al.*[23] Rovibrational levels are labeled with the bent molecule vibrational quantum number v_2 and with the rotational quantum numbers N, K, δ, where N is the quantum number of the total value of the rotational angular momentum, $K \geq 0$ corresponds to the eigenvalue of its molecule-fixed component N_z, and $\delta = \pm 1$. In the case of CH_2, $K = K_a$ and $K_a + K_c$ is N and $N+1$ when δ is +1 and −1, respectively. The symmetry species of the levels should be retrieved using Table I.

Table I. Symmetry species of rovibrational wavefunctions[a]

	δ		N	
K[b]	v_3 even	v_3 odd	even	odd
e	+1	−1	A_1	B_1
e	−1	+1	B_1	A_1
o	+1	−1	A_2	B_2
o	−1	+1	B_2	A_2

[a] C_{2v} symmetry species of symmetry adapted wavefunctions labeled by the rotational quantum numbers N, K, δ of Coudert *et al.*[23] and the vibrational quantum number v_3. The latter should be ignored and the column headed 'v_3 even' used for symmetry adapted wavefunctions in Section III B.
[b] The symbols e and o stand for even and odd, respectively.

For the cation, the Renner-Teller effect is accounted for as in Section III B of Coudert *et al.*[23] where the C_s symmetry labels A' and A'' of the Renner-Teller substates should be replaced by those appropriate for CH_2^+, A_1 and B_1, respectively. An increased accuracy is achieved taking two different γ-dependent reference configurations for the Renner-Teller substates. Two generalized inverse inertia tensors, denoted $\boldsymbol{\mu}^A(t)$ and $\boldsymbol{\mu}^B(t)$ for respectively the A_1 and B_1 substates, then arise and several equations of Coudert *et al.*[23] should be altered. In their Eq. (13),

the nondiagonal term $V_-(t)$ should be replaced by:

$$H_-^{\Lambda,N,k} = \tfrac{1}{2}P_t\mu_{tt}^-(t)P_t + k\Lambda\mu_{zz}^-(t) + \tfrac{1}{4}[N(N+1)-k^2][\mu_{xx}^-(t)+\mu_{yy}^-(t)] + V_-(t), \quad (2)$$

where $\mu_{\delta\delta}^-(t)$, with $\delta = t, x, y, z$, is expressed in terms of diagonal components of the two generalized inverse inertia tensors as $[\mu_{\delta\delta}^A(t) - \mu_{\delta\delta}^B(t)]/2$; and $V_-(t) = [V^A(t) - V^B(t)]/2$ involves the bending potentials of the A_1 and B_1 substates. In Eqs. (14) and (15) of Coudert *et al.*,[23] the diagonal components $\mu_{\delta\delta}(t)$ should be replaced by $\mu_{\delta\delta}^+(t) = [\mu_{\delta\delta}^A(t) + \mu_{\delta\delta}^B(t)]/2$. The changes described by Eq. (2) do not lead to additional singularities as $\mu_{tt}^-(t)$, $\mu_{xx}^-(t)$, $\mu_{yy}^-(t)$, and $\mu_{zz}^-(t)$ go to zero for the linear configuration. This allows us to setup and diagonalize the Renner-Teller Hamiltonian as in Coudert *et al.*[23] and $n_{\mathrm{Max}} = 33$, $\alpha^{\pm} = 12$, and $P = 34$ were taken. Symmetry adapted rovibronic wavefunctions in the case of the C_{2v} symmetry group can be retrieved from Eq. (17) of Coudert *et al.*[23] Their symmetry species should be retrieved from Table I. The rovibronic levels arising from each Renner-Teller substate can be labeled with the bent molecule vibrational quantum number v_2 and with the rotational quantum numbers N, K, δ.

The present calculation yields a theoretical value of 10.3645 eV for the adiabatic ionization potential which is 0.022 eV below that retrieved by Willitsch *et al.*[5] Table II displays a comparison between the present rovibronic energies and previously calculated ones for levels belonging to the ground stretching state with $N = K = 0$ and 1. For CH_2, the present energies are compared with those of Jensen and Bunker[28] after averaging K-type doublet energies. For CH_2^+, the present energies are compared with those of Jensen *et al.*[30] after averaging also spin-orbit components energies. For CH_2, the discrepancies range from 2.5 to 80 cm^{-1}. For CH_2^+, the discrepancies are larger, especially for the $A^+\,^2B_1$ substate where they are on the order of 200 cm^{-1}.

Table II. Calculated rovibronic energies[a] of CH_2 and CH_2^+

State	v_2	N, K	Calc.[b]	*This work*[c]
$X\,^3B_1$	0	1	78.9	81.4
	1	0	963.1	975.0
	1	1	1132.7	1157.5
	2	0	1828.5	1848.3
	2	1	2195.5	2242.2
	3	0	2818.8	2874.1
	3	1	3349.5	3431.1
$X^+\,^2A_1$	0	1	76.3	68.8
	1	0	995.6	988.5
	1	1	962.1	923.8
	2	0	2093.1	2106.4
	2	1	1725.4	1690.5
	3	0	3327.1	3385.3
	3	1	2751.6	2768.6
$A^+\,^2B_1$	0	0	2980.1	2919.1
	0	1	4192.3	3978.0
	1	0	5350.0	5383.6
	1	1	6500.9	6574.5
	2	0	7699.1	7840.6
	2	1	8901.2	8735.8

[a] Levels are identified by their electronic state, the bent molecule vibrational quantum number v_2, and the rotational quantum numbers N and K, taken equal.
[b] Energy in cm^{-1} reported by Jensen and Bunker[28] for CH_2 and Jensen *et al.*[30] for CH_2^+.
[c] Energy in cm^{-1} calculated in Section III B.

C. Observed and calculated TPES

The threshold photoelectron spectrum is modeled using the results in Section IV B of Coudert *et al.*[23] The total photoionization cross section σ_{tot} for a transition belonging to the $X^+\,\Pi \leftarrow X\,\Sigma$ ionizing transition with upper and lower levels N^+, K^+, δ^+, v^+ and N'', K'', δ'', v'', respectively, takes the form:

$$\sigma_{\mathrm{tot}} = \rho''\left[(q_v^+)^2 \sum_{|\lambda''|\le l''} \frac{Q^+(l'')B_{l''\lambda''}^{(X)}}{2l''+1} + (q_v^-)^2 \sum_{|\lambda''|\le l''} \frac{Q^-(l'')B_{l''\lambda''}^{(X)}}{2l''+1}\right]/2, \quad (3)$$

where $B_{l''\lambda''}^{(X)}$ is the electronic term defined in Eq. (10) of Willitsch *et al.*;[36] ρ'' is a weighing factor depending on the lower level; $(q_v^{\pm})^2$ are Franck-Condon factors; $Q^{\pm}(l'')$ are angular factors; and l'' and λ'' are the angular momentum and its projection for the molecular orbital from which ionization occurs. The Franck-Condon factors take the following expression:

$$(q_v^{\pm})^2 = \left| \int_{-1}^{+1} \mathrm{d}t\, \psi_{v''}^{N'',K''}(t) \times \left[\psi_{v^+}^{+,N^+,K^+}(t) \pm \psi_{v^+}^{-,N^+,K^+}(t)\right]\right|^2, \quad (4)$$

and involve the vibrational functions of the neutral and cationic species. In Eq. (3), the angular factors $Q^{\pm}(l'')$ should be obtained from Eq. (20) of Coudert *et al.*[23] after making the change indicated in their Section IV B:

$$Q^{\pm}(l'') = (2N^+ + 1)\left[\begin{pmatrix} N^+ & l'' & N'' \\ -K^+ & \lambda'' & K'' \end{pmatrix} + \delta''\begin{pmatrix} N^+ & l'' & N'' \\ -K^+ & \lambda'' & -K'' \end{pmatrix} \pm \delta^+\begin{pmatrix} N^+ & l'' & N'' \\ K^+ & \lambda'' & K'' \end{pmatrix} \pm \delta^+\delta''\begin{pmatrix} N^+ & l'' & N'' \\ K^+ & \lambda'' & -K'' \end{pmatrix}\right]^2 / h(K^+, K''). \quad (5)$$

where $h(K^+, K'') = 4(1+\delta_{K^+,0})(1+\delta_{K'',0})$.

When using Eq. (3), the restrictions on the quantum numbers of the upper and lower levels due to the nature

of the partial wave describing the photoelectron should be taken into account.[36,37] When l the orbital quantum number of this partial wave is odd, the C_{2v} symmetry species of the upper and lower level should be the same. Table I emphasizes that K^+ and K'' should then have the same parity. When l is even, the product of the symmetry species should be A_2 and K^+ and K'' should then have opposite parity.

Since in CH_2 the photoelectron is ejected from a π_u orbital, λ'' should be set to 1 and the summation in Eq. (3) was restricted to the first $l'' = 1$ term. The photoionization cross sections were calculated adding the contributions of lines with $0 \leq v'' \leq 10$, $0 \leq v^+ \leq 25$, $0 \leq N'', N^+ \leq 25$, and $0 \leq K'', K^+ \leq 12$. The weighing factor ρ'' in Eq. (3) was evaluated assuming a Boltzmann equilibrium characterized by a temperature of 300 K. A nuclear spin statistical weight equal to 1 (3) was taken for lower levels belonging to the symmetry species A_1 or A_2 (B_1 or B_2). The orbital quantum number l of the photoelectron partial wave is assumed to be even.[36,37] A Gaussian line shape with a half width at half maximum of 137 cm^{-1} was taken for each individual line in agreement with Section II.

Observed and calculated TPES are plotted in Fig. 4. The calculated TPES displays a narrow feature where a K-type structure can easily be seen and a broad feature dominated by several Franck-Condon progressions. The three prominent ones correspond to transitions connecting rotational levels with $K'' = 0$ and 1 of the neutral ground vibrational state and rovibronic levels of the cation belonging to the $A^+\,^2B_1$ Renner-Teller substate with $0 \leq v_2^+ \leq 4$ and $0 \leq K^+ \leq 2$. A fourth progression, not drawn in Fig. 4, corresponds to transitions originating from levels with $K'' = 2$. This progression leads to a broadening of the bands calculated at 11.2, 11.5, and 11.8 eV.

Comparing observed and calculated spectra, we can see that there is an agreement between the widths of the narrow features, but the K-structure is not seen in the observed spectrum. Also, line positions and relative line intensities do not agree. Although there is an agreement between line positions for the six bands from 10.74 to 11.47 eV, this is not the case for the three remaining ones at 11.61, 11.75, and 11.89 eV with calculated counterparts characterized by too high energies of 11.64, 11.79, and 11.94 eV, respectively. The observed band near 10.74 eV, which is the strongest line of the broad feature, only has a weak counterpart in the calculated spectrum. Matching the position of the narrow features and accounting for the experimental field induced shift described in Section II, the experimental adiabatic ionization potential was found to be 10.385(6) eV where the 6 meV uncertainty accounts for the 4 meV measurement accuracy plus the 2 meV error of the matching process. This value of the adiabatic ionization potential is 1.4 meV below that retrieved by Willitsch *et al.*[5]

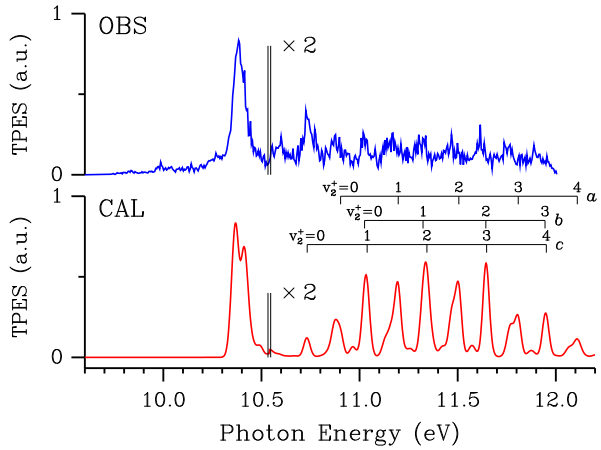

Figure 4. Observed (Calculated) TPES of the $X^+\,^2\Pi_u \leftarrow X\,^3B_1$ ionizing transition of CH_2 in the upper (lower) panel. The theoretical TPES was obtained using the bending model of Section III. The y-axes scales are multiplied by 2 for a photon energy larger than 10.54 eV. In the lower panel, Franck-Condon progression a originates from the neutral $v_2'' = K'' = 0$ level and connects the $v_2^+, K^+ = 1$ level of the cation $A^+\,^2B_1$ substate. Progressions b and c both originate from the neutral $v_2'' = 0, K'' = 1$ level and connect the $v_2^+, K^+ = 2$ and $K^+ = 0$ levels of the cation $A^+\,^2B_1$ substate, respectively. The value of the bent molecule vibrational quantum number v_2^+ appears in the figure.

IV. TRIDIMENSIONAL TREATMENT

The treatment described below can be used for calculating the TPES spectrum of a C_{2v} symmetry XY_2 neutral molecule with an $X\,\Sigma$ ground electronic state and an XY_2^+ cation with a Renner-Teller split $X^+\,\Pi$ ground electronic state. For the neutral, the approach of Gutle and Coudert[24] designed to solve the Schrödinger equation for a triatomic molecule is used to calculate the rovibronic energies. This approach is also used for the cation and the Renner-Teller effects are accounted for as in Mitrushchenkov.[25] The TPES is modeled adding both stretching modes in the treatment of Section III C. These results are applied to the water molecule and to CH_2.

A. Rovibronic energies of the neutral

The results of Section 3 of Gutle and Coudert[24] are used and the Hamiltonian is written using the Radau[38,39] stretching coordinates R_1 and R_2, and the bending coordinate $t = \cos\tilde{\gamma}$, where $\tilde{\gamma}$ is the Radau bending angle. The molecule-fixed axis system is attached to the molecule as in Gutle and Coudert[24] and the exact Hamiltonian, given in their Eqs. (5)–(8), is written:

$$K_{\rm vib} + V(R_1, R_2, t) + H_{\rm rot}, \qquad (6)$$

where $V(R_1, R_2, t)$ is the potential energy function; $H_{\rm rot}$ is the rotational Hamiltonian given in Eq. (8) of Gutle

and Coudert;[24] and $K_{\rm vib}$ is the vibrational kinetic energy:

$$K_{\rm vib} = \frac{P_{R_1}^2}{2m} + \frac{P_{R_2}^2}{2m} + \frac{1}{2m}\left(\frac{1}{R_1^2} + \frac{1}{R_2^2}\right) P_t(1-t^2)P_t, \quad (7)$$

where m is the mass of the Y terminal atom; and P_{R_1}, P_{R_2}, and P_t are conjugated momenta to R_1, R_2, and t, respectively. As in Section III B, rovibronic energies are calculated ignoring the spin-rotation and hyperfine couplings, and the asymmetry doubling. The rotational function is therefore taken as a symmetric top rotational function $|N,k\rangle$ characterized by N the quantum number of the total angular momentum and by k the eigenvalue of its molecule-fixed component N_z. The rotational Hamiltonian in Eq. (8) of Gutle and Coudert[24] can be replaced by its matrix element between too symmetric top rotational functions leading to:

$$H_{\rm rot}^{N,K}(X) = \frac{1}{2m}\left(\frac{1}{R_1^2} + \frac{1}{R_2^2}\right) \times \left[\frac{X^2}{2(1+t)} + [N(N+1) - K^2]\left(\frac{1}{4(1-t)} + \frac{1}{8}\right)\right], \quad (8)$$

where $K = |k|$. Rovibrational energies for each value of N and k are then obtained solving the Schrödinger equation for the vibrational Hamiltonian:

$$K_{\rm vib} + V(R_1, R_2, t) + H_{\rm rot}^{N,K}(K). \quad (9)$$

Vibrational energies and eigenfunctions are computed as outlined in Section 3 of Gutle and Coudert.[24] The parameters γ and δ describing the basis set bending functions in Eq. (12) of this reference are respectively set to $\sqrt{[N(N+1)-K^2]/2}$ and K in order to account for the singularities in the vibrational operator $H_{\rm rot}^{N,K}(K)$ of Eq. (8) for the $t = -1$ linear and $t = +1$ folded configurations. The parameters ξ and ρ describing the basis set stretching functions in Eq. (11) of Gutle and Coudert[24] depend on the potential energy function $V(R_1, R_2, t)$ and can be obtained using Eqs. (A4) and (A5) of Partridge and Schwenke[26] once the Radau bending coordinate t is set to its equilibrium value. Rovibronic energies and eigenfunctions take the form:

$$E(v_1, v_2, v_3, N, K) \quad \text{and} \quad \psi_{v_1,v_2,v_3}^{N,K}(R_1, R_2, t)|N, k\rangle, \quad (10)$$

where v_1 and v_3 are the usual vibrational quantum numbers for the symmetrical and antisymmetrical stretching modes, respectively; and v_2 is the bent molecule quantum number. Using the Wang-type rotational wavefunction in Eq. (10) of Coudert *et al.*,[23] symmetry adapted wavefunctions can be built:

$$\Psi^{v,N,K,\delta} = \psi_v^{N,K}(R_1, R_2, t)|NK\delta\rangle, \quad (11)$$

where v is a shorthand notation for v_1, v_2, v_3. Their symmetry species can be obtained from Table I. As stressed in Section III B, the usual rotational quantum number K_a is equal to K and K_c can be deduced from δ.

Table III. Calculated rovibronic energies[a] of CH_2

(v_1, v_2, v_3)	N	K	Calc.[b]	*This work*[c]
(0, 0, 0)	1	0	15.6	15.6
	1	1	78.9	78.9
(0, 1, 0)	0	0	963.1	963.4
	1	0	978.6	978.9
	1	1	1132.7	1132.7
(0, 2, 0)	0	0	1828.5	1829.0
	1	0	1843.9	1844.5
	1	1	2195.5	2195.6
(0, 3, 0)	0	0	2818.8	2818.2
	1	0	2834.5	2834.0
	1	1	3349.6	3349.5
(1, 0, 0)	0	0	2992.0	2992.3
	1	0	3007.4	3007.7
	1	1	3066.9	3067.0
(0, 0, 1)	0	0	3213.5	3213.6
	1	0	3228.9	3229.0
	1	1	3286.0	3286.2
(1, 1, 0)	0	0	3957.8	3949.7
	1	0	3973.1	3965.1
	1	1	4120.1	4120.2
(0, 4, 0)	0	0	4000.0	4006.7
	1	0	4015.8	4022.6
	1	1	4614.3	4614.3
(0, 1, 1)	0	0	4193.2	4192.8
	1	0	4208.4	4208.1
	1	1	4337.8	4337.9

[a] Levels are identified by the bent molecule vibrational quantum number v_2, the stretching vibrational quantum numbers v_1 and v_3, and the rotational quantum numbers N and K. The asymmetry doubling is neglected.
[b] Energy in cm^{-1} reported by Jensen and Bunker.[28]
[c] Energy in cm^{-1} calculated in Section IV A.

In the case of both the water molecule and CH_2, $v_{\rm Max}^t = 21$ and $v_{\rm Max}^r = 15$ were taken. In the case of the water molecule, the potential energy function $V(R_1, R_2, t)$ was obtained from Partridge and Schwenke.[26] In the case of CH_2, the potential energy function was evaluated with the help of Eqs. (1)–(3) of Jensen and Bunker,[28] taking the fitted parameters in their Table II. In the case of both molecules, Eqs. (2.21) and (2.22) of Johnson and Reinhardt[39] were used to transform from the Radau coordinates to the usual stretching and bending coordinates. For the water molecule, rovibrational energies were calculated up to the (002) vibrational states and are within 0.5 cm^{-1} from those of Partridge and Schwenke[26] for $N = K = 0$. For CH_2, Table III displays a comparison between the rovibronic energies of Jensen and Bunker[28] and those calculated in this work. For $K = 1$, as in Section III B, the average of the K-type doublet energies of Jensen and Bunker[28] was taken. Both sets of energies agree within better than 1 cm^{-1}, except for the close lying $(1, 1, 0)$ and $(0, 4, 0)$ states displaying discrepancies of approximately ± 8 cm^{-1} for $K = 0$.

B. Rovibronic energies of the cation

The vibronic Hamiltonian is obtained from Section II of Mitrushchenkov[25] using the x-embedding and Radau[38,39] coordinates. The Renner-Teller effect leads to A_1 and B_1 electronic substates with potential energy functions denoted $V^A(R_1,R_2,t)$ and $V^B(R_1,R_2,t)$, respectively. For a given value of the rotational quantum numbers N and K, the vibronic wavefunction is written:

$$|+\Lambda\rangle\chi_v^{+,N,K}(R_1,R_2,t)+|-\Lambda\rangle\chi_v^{-,N,K}(R_1,R_2,t), \quad (12)$$

where $|\pm\Lambda\rangle$ are electronic wavefunctions which are eigenfunctions of L_z with eigenvalues $\pm\Lambda$ in the linear limit; and $\chi_v^{\pm,N,K}(R_1,R_2,t)$ are vibrational functions identified by the three vibrational quantum numbers v_1,v_2,v_3 indicated by the shorthand notation v. The Hamiltonian for these two functions, from Eq. (13) of Mitrushchenkov,[25] is the 2×2 matrix operator given below:

$$(K_{\rm vib}+W^+)I+\begin{pmatrix} H_{\rm rot}^{N,K}(K-\Lambda) & W^- \\ W^- & H_{\rm rot}^{N,K}(K+\Lambda)\end{pmatrix}, \quad (13)$$

where I is the 2×2 identity matrix; $K_{\rm vib}$ and $H_{\rm rot}^{N,K}(X)$ are defined in Eqs. (7) and (8), respectively; and $W^\pm$ are potential energy terms equal to $[V^A(R_1,R_2,t)\pm V^B(R_1,R_2,t)]/2$.

The $\chi_v^{\pm,N,K}(R_1,R_2,t)$ vibrational functions are expanded using the basis set functions in Eqs. (9)–(12) of Gutle and Coudert.[24] The parameters $\gamma^\pm$ and $\delta^\pm$ describing the bending basis set functions are set respectively to $\sqrt{[N(N+1)-K^2]/2}$ and $|K\pm\Lambda|$ in order to account for the singularities of the vibrational operator $H_{\rm rot}^{N,K}(K\pm\Lambda)$ in Eq. (13). The parameters ξ and ρ describing the stretching basis set functions should be retrieved as in Section IV A using the W^+ potential energy functions and setting the Radau bending coordinate t to the value minimizing W^+. Setting-up the matrix of the Hamiltonian in Eq. (13) requires evaluating matrix elements of W^-. As the $\chi_v^{+,N,K}(R_1,R_2,t)$ and $\chi_v^{-,N,K}(R_1,R_2,t)$ vibrational functions are expanded using bending basis set functions characterized by a different value of δ, Eq. (A1) should be utilized.

Based on Eq. (17) of Coudert *et al.*,[23] symmetry adapted rovibronic wavefunctions can be built:

$$\begin{aligned}\Psi^{v,\Lambda,N,K,\delta} = \{&|A'\rangle\,[\chi_v^+ + \chi_v^-]\,|NK\delta\rangle \\ &+ i|A''\rangle[\chi_v^+ - \chi_v^-]|NK-\delta\rangle\}/\sqrt{2},\end{aligned} \quad (14)$$

where $\chi_v^\pm$ is a shorthand notation for the vibrational functions $\chi_v^{\pm,N,K}(R_1,R_2,t)$ in Eq. (12). Table I should be used to obtain the symmetry species of the rovibronic wavefunctions in Eq. (14). In agreement with this equation, the levels arising from each Renner-Teller substate are labeled using the three vibrational quantum numbers (v_1,v_2,v_3) and the rotational quantum numbers N,K,δ. As in Jensen *et al.*,[30] v_2 is the bent molecule vibrational quantum number. This quantum number was defined differently by Wang *et al.*[17] who used the linear molecule notation.

Table IV. Calculated vibronic energies[a] of H_2O^+

State	(v_1,v_2,v_3)	Calc.[b]	*This work*[c]
$X^+\,^2B_1$	(0, 1, 0)	1417.8	1418.3
	(0, 2, 0)	2784.4	2785.4
	(1, 0, 0)	3209.5	3212.5
	(0, 0, 1)	3255.2	3258.4
	(0, 3, 0)	4097.3	4098.7
	(0, 4, 0)	5351.9	5353.6
	(0, 5, 0)	6552.2	6554.3
	(0, 6, 0)	7732.5	7735.2
	(0, 7, 1)	8950.7	8953.9
	(0, 8, 0)	10240.2	10244.1
	(0, 9, 0)	11601.3	11604.1
	(0, 10, 0)	13021.8	13027.7
$A^+\,^2A_1$	(0, 0, 0)	8416.8	8418.2
	(0, 1, 0)	9922.0	9923.7
	(0, 2, 0)	11601.7	11606.2
	(0, 3, 0)	13408.0	13410.9
	(0, 4, 0)	15301.2	15304.9
	(0, 5, 0)	17261.7	17266.2
	(0, 6, 0)	19276.2	19281.0

[a] Vibronic states are identified by their electronic state, the bent molecule vibrational quantum number v_2, and the stretching vibrational quantum numbers v_1 and v_3.
[b] Energy in cm^{-1} reported by from Wu *et al.*[27]
[c] Energy in cm^{-1} calculated in Section IV B.

Vibronic energies of H_2O^+ and CH_2^+ were calculated taking $v_{\rm Max}^t=15$ and $v_{\rm Max}^r=17$. For H_2O^+, the potential energy terms W^+ and W^- in Eq. (13) were obtained from Wu *et al.*[27] For CH_2^+, these potential energy terms were obtained using Eqs. (1)–(5) of Kraemer *et al.*[29] with the parameters in Table 1 of Bunker *et al.*[31] Parameters $f_0^{(1,-)}$ and $f_{13}^{(0)}$ were set to -9883.7 and -1310.7 cm^{-1}, respectively, the values determined through adjustment by these authors. Tables IV and V display a comparison between the vibronic energies calculated in this work and those of Wu *et al.*[27] and Bunker *et al.*[31] for H_2O^+ and CH_2^+, respectively. Both sets of energies agree within better than 10 and 5 cm^{-1} for the former and latter molecules, respectively. Since calculated rovibronic energies are not reported for the upper $A^+\,^2B_1$ electronic substate of CH_2^+ in Bunker *et al.*,[31] the calculated energy for this substate in Table V were taken from Jensen *et al.*[30] and their energy was computed in this work using the parameters in in Table 1 of Kraemer *et al.*[29] and accounting for the correction in Section II of Jensen *et al.*[30]

C. TPES modeling

The results of Section III C are extended to include the two stretching modes. The expressions of the total photoionization cross section $\sigma_{\rm tot}$ in Eq. (3) and of the

Table V. Calculated vibronic energies[a] of CH_2^+

State	(v_1, v_2, v_3)	Calc.[b]	*This work*[c]
$X^+\,^2A_1$	(0, 1, 0)	997.0	997.0
	(0, 2, 0)	2102.2	2102.4
	(1, 0, 0)	2899.5	2899.4
	(0, 0, 1)	3131.6	3131.5
	(0, 3, 0)	3346.4	3346.4
	(1, 1, 0)	3888.6	3889.0
	(0, 1, 1)	4111.9	4112.3
	(0, 4, 0)	4701.0	4701.0
	(1, 2, 0)	4986.8	4987.9
	(0, 2, 1)	5187.7	5188.7
	(2, 0, 0)	5736.4	5735.8
	(1, 0, 1)	5923.4	5922.6
	(0, 5, 0)	6114.7	6115.2
	(0, 0, 2)	6202.4	6202.4
	(1, 3, 0)	6251.6	6252.7
	(0, 3, 1)	6397.2	6398.7
	(2, 1, 0)	6717.1	6717.8
	(1, 1, 1)	6894.9	6895.5
$A^+\,^2B_1$	(0, 0, 0)	2980.1	2980.7
	(0, 1, 0)	5350.0	5350.6
	(1, 0, 0)	5866.3	5867.9
	(0, 0, 1)	6130.2	6131.8
	(0, 2, 0)	7699.1	7699.9
	(1, 1, 0)	8212.3	8215.2
	(0, 1, 1)	8443.9	8446.7
	(2, 0, 0)	8689.2	8692.5
	(1, 0, 1)	8906.2	8909.7
	(0, 0, 2)	9219.9	9223.4
	(0, 3, 0)	10028.4	10029.5
	(1, 2, 0)	10536.1	10540.2
	(0, 2, 1)	10736.8	10740.7

[a] Vibronic states are identified by their electronic state, the bent molecule vibrational quantum number v_2, and the stretching vibrational quantum numbers v_1 and v_3.
[b] Energy in cm^{-1} reported by Bunker *et al.*[31] for the $X^+\,^2A_1$ substate and by Jensen *et al.*[30] for the $A^+\,^2B_1$ substate.
[c] Energy in cm^{-1} calculated in Section IV B. For the $A^+\,^2B_1$ substate, the parameters of Kraemer *et al.*[29] and Jensen *et al.*[30] were used.

angular factors $Q^{\pm}(l'')$ in Eq. (5) do not need to be modified. The Franck-Condon factors $(q_v^{\pm})^2$ in Eq. (4) should be rewritten as:

$$(q_v^{\pm})^2 = \left| \iiint \mathrm{d}R_1\,\mathrm{d}R_2\,\mathrm{d}t\,\psi_{v''}^{N'',K''}(R_1,R_2,t) \times \left[\chi_{v^+}^{+,N^+,K^+}(R_1,R_2,t) \pm \chi_{v^+}^{-,N^+,K^+}(R_1,R_2,t)\right] \right|^2, \quad (15)$$

and involve the vibrational function of the neutral in Eq. (11) and those of the cation in Eq. (14). The integral over vibrational coordinates can be evaluated using Eqs. (A1) and (A2) since the vibrational function of the neutral and the cation are expanded with basis set functions of Gutle and Coudert[24] characterized by different values of γ, δ, ξ, and ρ.

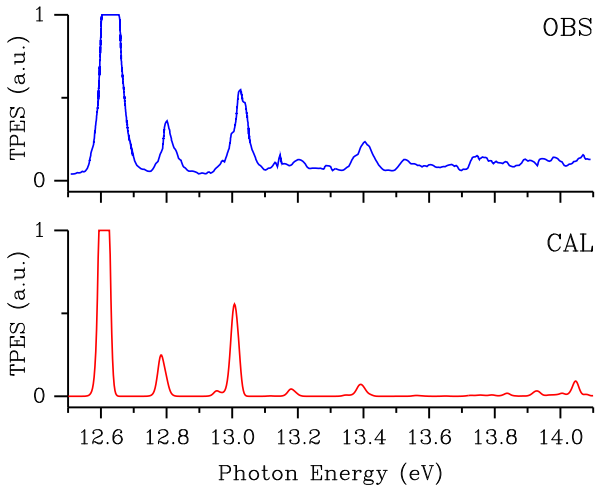

Figure 5. Experimental and simulated TPES of the $X^+\,^2B_1 \leftarrow X\,^1A_1$ ionizing transition of H_2O are plotted in the upper and lower panels, respectively. The experimental TPES was taken from Fig. 3 of Truong *et al.*[40] The theoretical TPES was obtained using the tridimensional treatment of Section IV.

D. Observed and calculated TPES

In the case of the water molecule, just as in CH_2, the photoelectron is ejected from a π_u orbital. As in Section III C, λ'' is set to 1 and the summation in Eq. (3) is restricted to the first $l'' = 1$ term. The TPES were calculated adding the contribution in Eq. (3) from lines with $0 \le N'', N^+ \le 20$ and $0 \le K'', K^+ \le 12$. The weighing factor ρ'' was evaluated as in Section III C and the orbital quantum number l of the photoelectron partial wave was assumed to be even.[36,37]

Observed and calculated TPES for the water molecule are plotted in Fig. 5 for the $X^+\,^2B_1 \leftarrow X\,^1A_1$ ionizing transition and in Fig. 6 for the $A^+\,^2A_1 \leftarrow X\,^1A_1$ ionizing transition. The observed TPES was taken from Truong *et al.*[40] for both figures. The calculated TPES were computed assuming a temperature of 300 K and a Gaussian line shape with a half width at half maximum of 70 cm^{-1}. This leads to a reasonable agreement with the experimental spectra.

Assuming a temperature of 300 K and a Gaussian line shape with a half width at half maximum of 137 cm^{-1}, as in Section III C, the TPES of CH_2 was computed and is compared with the experimental spectrum in Fig. 7. As in Fig. 4, the calculated spectrum displays a broad feature dominated by Franck-Condon progressions due to the bending mode. The spectrum calculated in this section is, however, closer to the experimental spectrum. For the broad feature, a better agreement for line positions can be seen, especially for the three high energy bands at 11.61, 11.75, and 11.89 eV. A more satisfactory agreement also arises for relative line intensities. The observed line near 10.74 eV has a stronger counterpart in the calculated spectrum. Shifting the theoretical spec-

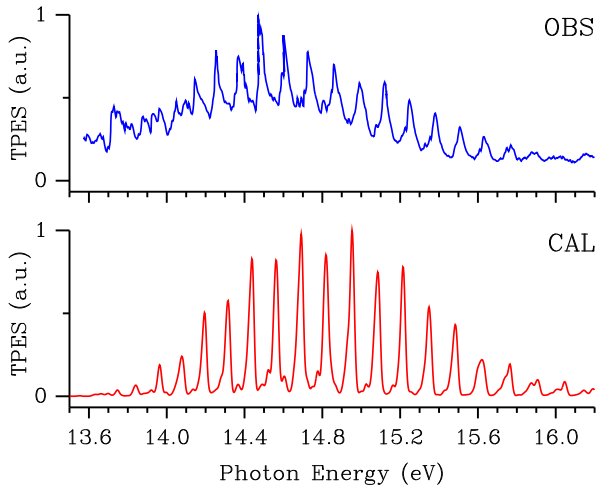

Figure 6. Experimental and simulated TPES of the $A^+\,^2A_1 \leftarrow X\,^1A_1$ ionizing transition of H_2O are plotted in the upper and lower panels, respectively. The experimental TPES was taken from Fig. 4 of Truong *et al.*[40] The theoretical TPES was obtained using the tridimensional treatment of Section IV.

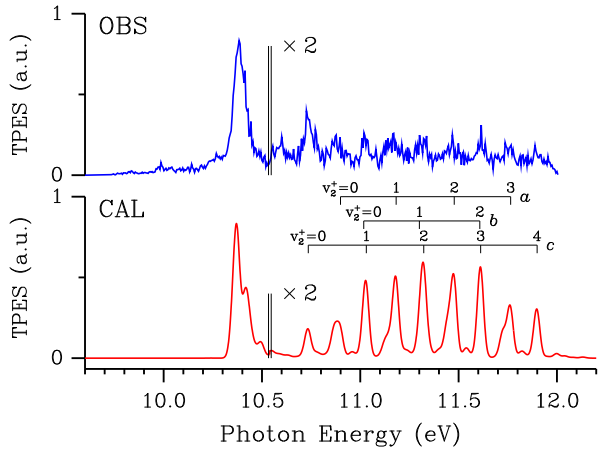

Figure 7. Observed (Calculated) TPES of the $X^+\,^2\Pi_u \leftarrow X\,^3B_1$ ionizing transition of CH_2 in the upper (lower) panel. The theoretical TPES was obtained using the tridimensional treatment of Section IV. The y-axes scales are multiplied by 2 for a photon energy larger than 10.54 eV. In the lower panel, Franck-Condon progression a originates from the neutral $(000), K'' = 0$ level and connects the $(0v_2^+0), K^+ = 1$ level of the cation $A^+\,^2B_1$ substate. Progressions b and c both originate from the neutral $(000), K'' = 1$ level and connect the $(0v_2^+0), K^+ = 2$ and $K^+ = 0$ level of the cation $A^+\,^2B_1$ substate, respectively. The value of the bent molecule vibrational quantum number v_2^+ is given in the figure.

trum so as to obtain the best match with the experimental one, the experimental value obtained for the adiabatic ionization potential was found to be 10.386(6) eV, accounting for the experimental field induced shift and estimating the uncertainty as in Section III C. This new experimental value of the adiabatic ionization potential is more reliable than that obtained in Section III C and is 0.4 meV below that retrieved by Willitsch *et al.*[5]

V. DISCUSSION

The TPES of the $X^+\,^2\Pi_u \leftarrow X\,^3B_1$ ionizing transition of methylene has been recorded in this investigation with the experimental setup described in Section II. This spectrum is analyzed with a previously developed bending model[23] and a new model presented in this work. Both approaches allow us to model the TPES of the $X^+\,\Pi \leftarrow X\,\Sigma$ ionizing transition of a C_{2v} symmetry molecule where the $X^+\,\Pi$ electronic state of the cation is Renner-Teller split.

The bending model[23] relies on *ab initio* bending potentials retrieved in this work for CH_2 and presented in Section III A. The new model, designed for triatomic molecules, is described in Section IV and is based on the exact Hamiltonian[24] of a triatomic molecule written using Radau Coordinates.[38,39] The Renner-Teller coupling in the $X^+\,\Pi$ electronic state is treated as in Mitrushchenkov.[25]

The new model is first tested in the case of the $X^+\,^2\Pi_u \leftarrow X\,^1A_1$ ionizing transition of the water molecule using tridimensional potential energy surfaces[26,27] for H_2O and H_2O^+. The theoretical TPES, shown in Figs. 5 and 6, compares well with the experimental one.[40] In the case of CH_2, the TPES is computed using tridimensional potential energy surfaces[28,31] for CH_2 and CH_2^+.

The TPES of the $X^+\,^2\Pi_u \leftarrow X\,^3B_1$ ionizing transition of CH_2 calculated with the bending model[23] and the new model are shown in Figs. 4 and 7, respectively, where they are compared with the experimental TPES. Both treatments lead to a theoretical spectrum dominated by Franck-Condon progressions due to the large amplitude bending mode. Although both theoretical spectra are qualitatively similar, a much better agreement with the experimental spectrum is achieved with the new model for line positions. For relative line intensities, however, the agreement with the experimental data is not satisfactory for both treatments, especially for the high energy region of the spectrum.

The *ab initio* bending potentials and the bending model[23] lead to a value of 10.3645 eV for the adiabatic ionization potential which, as stressed in Section III B, is 0.022 eV below that retrieved by Willitsch *et al.*[5] The comparison between observed and calculated TPES carried out in Section III C in the case of the bending model[23] leads to a larger value of 10.385(6) eV which is 1.4 eV below that retrieved by Willitsch *et al.*[5] The comparison carried out in Section IV D using the new model leads to the a slightly larger value of 10.386(6) eV, which is our preferred value. It is only 0.4 meV below that retrieved by Willitsch *et al.*[5] and agrees within experimental uncertainty with their value. The satisfactory agreement for the adiabatic ionization potential and for the line positions of the TPES suggests that the accu-

racy achieved with the tridimensional potential energy surfaces[28,31] used for CH_2 and CH_2^+ is satisfactory.

The main issue of the present investigation is the intensity of the TPES lines. More precisely the discrepancy between experimental and theoretical TPES for the intensity ratio between the narrow isolated feature at 10.38 eV and the broad feature spanning the 10.6 to 12 eV energy range. This discrepancy may be due to experimental and theoretical reasons.

With the experimental setup used in this investigation, the population of the methylene energy levels is not known accurately as it is a reactive species produced through hydrogen atom abstractions. This may result in a cell temperature differing substantially from the room temperature selected for Figs. 4 and 7. The theoretical TPES of CH_2 presented in these figures were recalculated for a lower temperature of 200 K and a higher one of 400 K. Although changes of the theoretical TPES were observed, they were not large enough to account for the intensity ratio discrepancy.

As pointed out in previous investigations of unstable species,[33,41,42] line intensities should be modeled using a non Boltzmannian equilibrium with a high vibrational temperature and a lower rotational temperature. Although this might explain the intensity ratio discrepancy, applying these ideas to methylene is not straightforward. Due to the quasilinearity, rotation about the a axis leads to rotational energies which are no longer small compared to the vibrational spacing. Table II emphasizes that the energy difference between the $K = 1$ and 0 rotational levels is 530.7 cm^{-1} for $v_2 = 3$ which is not small compared to the fundamental frequency of the ν_2 mode, 963.1 cm^{-1}.

In the theoretical line intensity calculation, the electronic terms $B^{(X)}_{l''\lambda''}$ introduced by Willitsch *et al.*[36] and appearing in Eq. (3) of the present paper were assumed to be constants independent on the stretching coordinates and on the bending angle γ. In the case of non-rigid molecules like methylene and its cation CH_2^+, characterized by a low barrier to linearity, the bending wavefunction samples a large angular range and adding a dependence of the $B^{(X)}_{l''\lambda''}$ electronic terms on the angle γ might lead to significant changes of the line intensity. *Ab initio* calculations, outside of the scope of the present paper, are needed to confirm this assumption. Perturbations to the intensity of the lines in a TPES may also be due to autoionization. This effect, shown to be important in the CH radical,[33] was ignored in the theoretical modeling.

Appendix A: Basis set functions and matrix elements

The bending basis set functions $v_m^{\gamma\delta}(t)$ in Eq. (12) of Gutle and Coudert[24] are identical to the $\theta_n^{\alpha\beta}(t)$ in Eq. (4) of Coudert *et al.*[23] provided $\alpha = \gamma$ and $\beta = \delta$. Matrix elements of an $F(t)$ function between two such basis set functions:

$$\langle v_n^{\gamma_1\delta_1}|F(t)|v_m^{\gamma_2\delta_2}\rangle, \tag{A1}$$

should be calculated using the Gauss-Jacobi quadrature suited for a weight function of the form $(1-t)^\gamma(1+t)^\delta$ with $\gamma = (\gamma_1+\gamma_2)/2$ and $\delta = (\delta_1+\delta_2)/2$.

Evaluation of the matrix element of an $F(R)$ function between two stretching basis set functions $u_n^{\rho\xi}(R)$ in Eq. (11) of Gutle and Coudert[24]:

$$\langle u_n^{\rho_1\xi_1}|F(R)|u_m^{\rho_2\xi_2}\rangle, \tag{A2}$$

should be carried out using the Gauss-Laguerre quadrature suited for a weight function of the form $x^\rho \exp(-x)$ with $x = \xi R$, $\rho = (\rho_1+\rho_2)/2$, and $\xi^\rho = ({\xi_1}^{\rho_1/2} + {\xi_2}^{\rho_2/2})/2$.

ACKNOWLEDGMENTS

This work was performed on the DESIRS beamline under Proposal number 20140832. We thank SOLEIL for providing us with the synchrotron radiation facilities and the DESIRS beamline team for their assistance. We also thank Julia Krüger for her invaluable help in performing the experiments. This work received financial support from the French Agence Nationale de la Recherche (ANR) under Grant number ANR-12-BS08-0020-02 (project SYNCHROKIN). F. H. acknowledges funding by the Deutsche Forschungsgemeinshaft (DFG) through Grant Number FI 575/7-3 and the research training school GRK 2112. A. R. acknowledges funding through the research training school GRK 2112.

[1] G. Herzberg and J. Shoosmith, Nature **183**, 1801 (1959).
[2] G. Herzberg, Proc. R. Soc. London Ser. A **262**, 291 (1961).
[3] M. Litorja and B. Ruscic, J. Chem. Phys. **108**, 6748 (1998).
[4] B. Ruscic, M. Litorja, and R. L. Asher, J. Phys. Chem. A **103**, 8625 (1999).
[5] S. Willitsch, L. L. Imbach, and F. Merkt, J. Chem. Phys. **117**, 1939 (2002).
[6] S. Willitsch and F. Merkt, J. Chem. Phys. **118**, 2235 (2003).
[7] H. Ozeki and S. Saito, Astrophys. J. **451**, L97 (1995).
[8] E. A. Michael, F. Lewen, G. Winnewisser, H. Ozeki, H. Habara, and E. Herbst, Astrophys. J. **596**, 1356 (2003).
[9] S. Brünken, E. A. Michael, F. Lewen, T. Giesen, H. Ozeki, G. Winnewisser, P. Jensen, and E. Herbst, Can. J. Chem. **82**, 676 (2004).
[10] T. J. Sears, P. R. Bunker, A. R. W. McKellar, K. M. Evenson, D. A. Jennings, and J. M. Brown, J. Chem. Phys. **77**, 5348 (1982).
[11] T. J. Sears, J. Chem. Phys. **85**, 3711 (1986).
[12] M. D. Marshall and A. R. W. McKellar, J. Chem. Phys. **85**, 3716 (1986).
[13] S. Brünken, H. S. P. Müller, F. Lewen, and T. F. Giesen, J. Chem. Phys. **123**, 164315 (2005).
[14] G. Herzberg, Can. J. Phys. **39**, 1511 (1961).
[15] M. Rösslein, C. M. Gabrys, M.-F. Jagod, and T. Oka, J. Mol. Spectrosc. **153**, 738 (1992).
[16] J. L. Gottfried and T. Oka, J. Chem. Phys. **121**, 11527 (2004).
[17] H. Wang, C. F. Neese, C. P. Morong, M. Kleshcheva, and T. Oka, J. Phys. Chem. A **117**, 9908 (2013).

[18] G. A. Garcia, X. Tang, J.-F. Gil, L. Nahon, M. Ward, S. Batut, C. Fittschen, C. A. Taatjes, D. L. Osborn, and J.-C. Loison, J. Chem. Phys. **142**, 164201 (2015).
[19] G. A. Garcia, B. Gans, X. Tang, M. Ward, S. Batut, L. Nahon, C. Fittschen, and J.-C. Loison, J. Electron Spectrosc. and Relat. Phenom. **203**, 25 (2015).
[20] L. Nahon, N. de Oliveira, G. A. Garcia, J. Gil, B. Pilette, O. Marcouillé, B. Lagarde, and F. Polack, J. Synchrotron Rad. **19**, 508 (2012).
[21] N. L. Shinkle and J. Coon, J. Mol. Spectrosc. **40**, 217 (1971).
[22] S. Carter and N. C. Handy, J. Mol. Spectrosc. **95**, 9 (1982).
[23] L. H. Coudert, B. Gans, G. A. Garcia, and J.-C. Loison, J. Chem. Phys. **148**, 054302 (2018).
[24] C. Gutlé and L. H. Coudert, J. Mol. Spectrosc. **273**, 44 (2012).
[25] A. O. Mitrushchenkov, J. Chem. Phys. **136**, 024108 (2012).
[26] H. Partridge and D. W. Schwenke, J. Chem. Phys. **106**, 4618 (1997).
[27] S. Wu, Y. Chen, X. Yang, Y. Guo, Y. Liu, Y. Li, R. J. Buenker, and P. Jensen, J. Mol. Spectrosc. **225**, 96 (2004).
[28] P. Jensen and P. R. Bunker, J. Chem. Phys. **89**, 1327 (1988).
[29] W. P. Kraemer, P. Jensen, and P. R. Bunker, Can. J. Phys. **72**, 871 (1994).
[30] P. Jensen, M. Brumm, W. P. Kraemer, and P. R. Bunker, J. Mol. Spectrosc. **172**, 194 (1995).
[31] P. R. Bunker, W. P. Kraemer, S. N. Yurchenko, W. Thiel, C. F. Neese, J. L. Gottfried, and P. Jensen, Mol. Phys. **105**, 1369 (2007).
[32] G. A. Garcia, B. K. de Miranda, M. Tia, S. Daly, and L. Nahon, Rev. Sci. Instrum. **84**, 053112 (2013).
[33] B. Gans, F. Holzmeier, J. Krüger, C. Falvo, A. Röder, A. Lopes, G. A. Garcia, C. Fittschen, J.-C. Loison, and C. Alcaraz, J. Chem. Phys. **144**, 204307 (2016).
[34] H.-J. Werner, P. J. Knowles, G. Knizia, F. R. Manby, M. Schütz, and Others, "Molpro, version 2012.1, a package of ab initio programs," (2012).
[35] H.-J. Werner, P. J. Knowles, G. Knizia, F. R. Manby, and M. Schütz, Wiley Interdisciplinary Reviews: Computational Molecular Science **2**, 242 (2012).
[36] S. Willitsch and F. Merkt, Int. J. Mass Spec. **245**, 14 (2005).
[37] R. Signorell and F. Merkt, Mol. Phys. **92**, 793 (1997).
[38] R. Radau, Ann. Sci. Ecole Normale Supérieure **5**, 311 (1868).
[39] B. R. Johnson and W. P. Reinhardt, J. Chem. Phys. **85**, 4538 (1986).
[40] S. Y. Truong, A. J. Yencha, A. M. Juarez, S. J. Cavanagh, P. Bolognesi, and G. C. King, Chem. Phys. **355**, 183 (2009).
[41] C. Romanzin, B. Gans, S. Douin, S. Boyé-Péronne, and D. Gauyacq, Chem. Phys. **351**, 77 (2008).
[42] B. K. Cunha de Miranda, C. Alcaraz, M. Elhanine, B. Noller, P. Hemberger, I. Fischer, G. A. Garcia, H. Soldi-Lose, B. Gans, L. A. Vieira Mendes, S. Boyé-Péronne, S. Douin, J. Zabka, and P. Botschwina, J. Phys. Chem. A **114**, 4818 (2010).